AGU PUBLICATIONS

Geochemistry, Geophysics, Geosystems

RESEARCH ARTICLE

10.1002/2016GC006333

Key Points:
- Geochemistry of authigenic carbonates and clay minerals are analyzed in central China
- The PETM was characterized by an overall increase in precipitation in China interior
- Geochemical proxies suggest an intensified continental weathering during the PETM

Supporting Information:
- Supporting Information S1
- Supporting Information S2

Correspondence to:
Z. Chen,
chenzl@mail.iggcas.ac.cn

Citation:
Chen, Z., Z. Ding, S. Yang, C. Zhang, and X. Wang (2016), Increased precipitation and weathering across the Paleocene-Eocene Thermal Maximum in central China, *Geochem. Geophys. Geosyst.*, *17*, doi:10.1002/2016GC006333.

Received 1 MAR 2016
Accepted 17 MAY 2016
Accepted article online 21 MAY 2016

Increased precipitation and weathering across the Paleocene-Eocene Thermal Maximum in central China

Zuoling Chen[1], Zhongli Ding[1], Shiling Yang[1], Chunxia Zhang[1], and Xu Wang[1]

[1]Key Laboratory of Cenozoic Geology and Environment, Institute of Geology and Geophysics, Chinese Academy of Sciences, Beijing, China

Abstract Global warming during the Paleocene-Eocene Thermal Maximum (PETM) ~55.5 million years ago (Ma) was associated with a massive release of carbon to the ocean-atmosphere system, as evidenced by a prominent negative carbon isotope excursion (CIE) and widespread dissolution of marine carbonates. The paleohydrologic response to the PETM warming has been studied worldwide; however, relevant records of environmental perturbation in Asia are lacking so far. Here we extend the record of this event in central China, a subtropical paleosetting, through geochemical and mineralogical analyses of lacustrine sediments. Geochemical indicators of authigenic carbonates—including molar Mg/Ca and Sr/Ca ratios—suggest an overall increased precipitation across the PETM, compatible with the disappearance of authigenic dolomite and the appearance of kaolinite in the strata. The relatively humid conditions persisted long after the carbon-cycle perturbation had stopped, implying that the transient hyper-greenhouse warming might have forced the regional climate system into a new climate state that was not easily reversed. Additionally, a gradual increase in chemical index of alteration (CIA) and the appearance of kaolinite are associated with the PETM, indicating an intensified silicate weathering and pedogenesis in the watershed in response to warmer and more humid climate. Our results corroborate the theory that an accelerated continental chemical weathering served as a negative feedback to sequester carbon and lower the atmospheric greenhouse-gas levels during the PETM.

1. Introduction

The Paleocene-Eocene Thermal Maximum (PETM; ~55.5 Ma) represents a period of geologically rapid, extreme global warming, superimposed on a long-term warming trend of the early Cenozoic [*Kennett and Stott*, 1991; *Zachos et al.*, 2008]. The onset of the event occurred within ~20 kyr and the total duration is estimated to be ~170 kyr [*Röhl et al.*, 2007; *Charles et al.*, 2011]. Existing records reveal that during the PETM, the Earth's surface temperature increased by at least 5°C globally [*Kennett and Stott*, 1991; *Thomas et al.*, 1999; *Zachos et al.*, 2003; *Tripati and Elderfield*, 2005], whereas stronger warming of up to 8°C has been reported locally at middle and high latitudes [*Sluijs et al.*, 2006; *Weijers et al.*, 2007; *Chen et al.*, 2014a]. Associated with the PETM are a globally recognized negative carbon isotope excursion (CIE) in sedimentary components of 2.5–8‰ [*Kennett and Stott*, 1991; *McInerney and Wing*, 2011; *Chen et al.*, 2014b] and a pervasive dissolution of deep-sea carbonates [*Zachos et al.*, 2005]. Collectively, these characteristics are consistent with the release of more than 2000 gigatons of isotopically depleted carbon into the ocean-atmosphere system [*Dickens et al.*, 1995; *Zachos et al.*, 2005; *Zeebe et al.*, 2009; *Meissner et al.*, 2014]. This is comparable in magnitude to that which could occur over the coming centuries. Therefore, the PETM has been proposed to be a geologically analogue for understanding anthropogenic climate change and for assessing the consequences of a rapid increase in atmospheric CO_2 concentrations.

Global warming is expected to exert a substantial effect on global and regional hydrological cycles [*Held and Soden*, 2006; *Trenberth*, 2011; *Pierrehumbert*, 2002; *Yang et al.*, 2015]. Model predictions for greenhouse-gas-driven warming indicate that on a global-scale evaporation and precipitation will increase [*Houghton et al.*, 2001]. Hydrological changes across the PETM have been investigated using various methodologies; however, the results have been inconsistent. High abundance of kaolinite, a product of weathering in warm, wet climate, and increased supply of terrigenous materials have been observed during the PETM in many marginal marine sites around the world [*Robert and Kennett*, 1994; *Bolle and Adatte*, 2001; *Hollis et al.*, 2005;

John et al., 2008]. These have generally been regarded as evidence for global increase in runoff or precipitation. Using soil-carbon cycle modeling, *Bowen et al*. [2004] also argue that the offset between the magnitude of the terrestrial and marine CIEs could be explained by potentially global increase in relative humidity. Yet most proxy data indicate that higher variability of precipitation in different regions during the PETM [*McInerney and Wing*, 2011]. Hydrogen isotope records of higher-plant leaf wax lipids are suggestive of increased precipitation in the Arctic [*Pagani et al*., 2006]. In contrast, mineralogical and sedimentological studies from northern Spain reflect seasonally wetter but generally dry conditions across the PETM [*Schmitz and Pujalte*, 2003, 2007]. In North America, paleosol and paleobotanical features provide evidence for a drier climate during the early PETM period but increasing precipitation in the later period [*Kraus and Riggins*, 2007; *Kraus et al*., 2013; *Wing et al*., 2005]. A more arid climate is also indicated by paleosols from the southern Rocky Mountains during the PETM [*Bowen and Bowen*, 2008]. In summary, available data suggest that substantial shifts in the hydrological cycle occurred during the PETM.

Another remaining outstanding question concerning the PETM is the fate of excess isotopically depleted carbon. The transient nature of the PETM (~170 kyr) and rapid removal of ^{12}C from the exogenic carbon reservoirs indicate that negative feedback mechanisms within the global carbon cycle were at work rapidly. One possibility is that global warming and increased precipitation during the PETM enhanced continental silicate-weathering reactions, thereby reduced greenhouse gas concentrations [*Zachos and Dickens*, 2000; *Zachos et al*., 2005]. The most compelling line of evidence for this mechanism is a prominent peak in the abundance of the clay mineral kaolinite of marginal marine sediments, which has been explained as intensified continental weathering [*Robert and Kennett*, 1994; *Kelly et al*., 2005]. This interpretation, however, is controversial because the kaolinite influx likely reflects deeper physical erosion of previously formed clay rather than intensified weathering during the geologically brief PETM [*Thiry and Dupuis*, 2000; *Schmitz et al*., 2001]. Therefore, more proxy data, especially those directly from continental sediments, are needed to tease out whether chemical weathering of silicate is enhanced.

To sum up, a wider geographical coverage of precipitation and weathering records is crucial for overall understanding climatic response to greenhouse-gas-induced warming during the PETM. However, relevant records of environmental perturbation in Asia are lacking so far. The recently recovered lacustrine PETM section (Beigou) in the Nanyang Basin, central China, provides the first opportunity to evaluate the Asian environmental response across the PETM. Here we have generated mineralogical and geochemical data through the lacustrine PETM sediments recovered from the Nanyang Basin [*Chen et al*., 2014a]. These new data have been used in an attempt to elucidate the hydrological and weathering response to the PETM warming in the subtropical continental settings.

2. Materials and Methods

2.1. Geological Setting

The Nanyang Basin (paleolatitude: ~31°N), situated in the eastern Qinling Mountain region, is a huge intermontane Mesozoic-Cenozoic down-faulted basin [*Feng et al*., 1997]. During the late Mesozoic, the collision between the North China and Yangtze plates brought about the uplift of the pre-Cretaceous strata to the south and new differentiation of crustal activity, including compressive folding and faulting throughout the area. Specially, the west part of the region uplifted significantly, while the east part subsided [*Wang et al*., 2003]. As a result, a large fault basin—Nanyang Basin—formed surrounding Nanyang during the late Cretaceous period, which received very thick alluvial-lacustrine deposits in the early Cenozoic (Figure 1a).

The late Cretaceous-early Eocene deposits at the basin are mostly developed and well exposed with clear stratigraphic sequences in north-west Hubei province, including the Hugang, Baiying, and Yuhuangding Formations in ascending order [*Feng et al*., 1999]. The Hugang Formation is predominately composed of reddish fine clastics, indicative of a shallow fluviolacustrine facies. The Baiying Formation dominated by thick lacustrine marls with interbedded calcareous mudstones. The overlying Yuhuangding Formation, marked by grayish-pink marls with interbedded reddish siltstones and calcareous mudstones, is interpreted as deep lacustrine facies environments. These thick marls and reddish siltstones, in combination with paleobiological and mineralogical records, demonstrate that this area was generally controlled by arid or semiarid climate during the early Cenozoic [*Sun and Wang*, 2005; *Guo et al*., 2008].

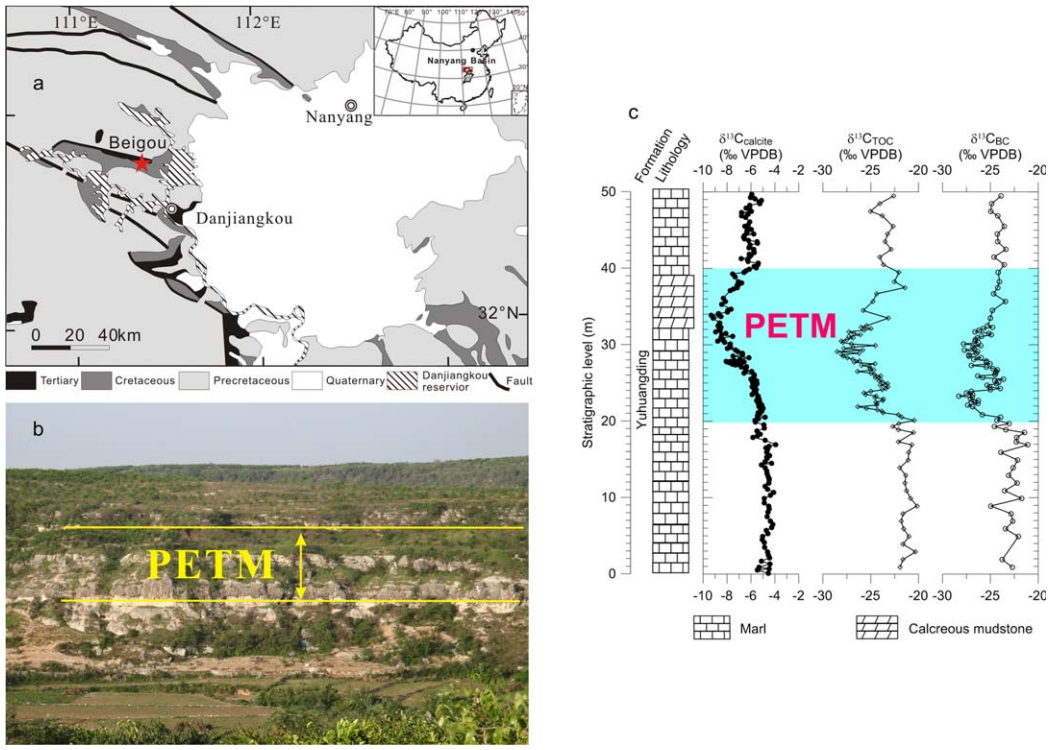

Figure 1. Geological backgrounds of the studied area. (a) Paleogeographic location and geological sketch map of the studied site. (b) Field photo of the PETM outcrop. (c) Stable carbon isotope ratios of calcite, total organic carbon (TOC), and black carbon (BC) from *Chen et al.* [2014a]. The red star shows the study site. The blue-shaded area highlights the PETM defined by multiproxy carbon isotope excursion.

In this study, we focus on the 50 m-thick lacustrine deposits in the lower part of the Yuhuangding Formation at the Beigou section (Beigou: 32°43.9′N, 111°27.6′E) (Figure 1a), which is close to the depocenter of the Basin. The Paleocene/Eocene transition at this section has previously been identified from biostratigraphy [*Ma and Cheng*, 1991; *Ting et al.*, 2003], and the PETM interval has been defined by a characteristic negative carbon isotope excursion recorded in the $\delta^{13}C$ values of both inorganic and organic substrates (Figure 1c) [*Zhu et al.*, 2010; *Chen et al.*, 2014a]. The complete PETM spans ~20 m stratigraphic interval from 20 to 40 m (Figure 1c). Paleotemperature reconstruction indicates that the continental temperatures rose ~7°C during the PETM in the Nanyang Basin; mean annual temperature (MAT) may have reached 31°C at the peak of the event [*Chen et al.*, 2014a].

2.2. Mineralogy and Element Analyses of Carbonates

The mineralogical compositions of 205 carbonate samples at the Beigou section have been determined by X-ray diffraction (XRD) in our previous study [*Chen et al.*, 2014a]. Carbonate concentrations in 112 solid samples were roughly determined gravimetrically by dissolving powered samples in 3 mol/L HCl, followed by filtration, drying, and weighing the insoluble residue.

Molar Mg/Ca and Sr/Ca ratios were obtained from selected carbonate samples (with an sample spacing of ~1 m) using inductively coupled-plasma optical-emission spectroscopy (ICP-OES) at the Institute of Geology and Geophysics, Chinese Academy of Sciences (IGG, CAS). An aliquot of powered sample was digested in 3 mol/L HCl, diluted with deionized water and filtered. Total dissolved Ca, Mg, and Sr were measured at wavelengths of 317.9, 279, and 407 nm, respectively. Replicate analyses of prepared blanks and standard solutions of varying known concentrations indicated detection limits for Ca, Mg, and Sr of 6, 2, and 0.1 μg/L, respectively, with precision better than 10 μg/L for Ca and Mg, and 1 μg/L for Sr.

2.3. Clay Mineral Measurements

Thirty-three samples were selected for clay mineral measurements. All samples were first disaggregated in distilled water and treated with 10% H_2O_2 and 2 mol/L acetic acid to remove organic matters and carbonates, respectively. The decarbonated suspensions were then washed successively with distilled water until

the suspensions were close to neutral to help the deflocculation of clays. The clays of <2 μm subfraction were separated from the suspension after a setting time calculated based on Stoke's law. Oriented mounts, including those saturated by $MgCl_2$, KCl, ethylene glycol (EG), and glycerol (G), were prepared by pipetting 1 mL of the aqueous clay suspension onto glass slides. X-ray diffraction analyses were performed using a PANAlytical diffractometer with Ni-filtered Cu-Kα radiation (40 kV, 40 mA) at the IGG, CAS.

Clay minerals were identified according to the position of the (001) series of basal reflections on XRD patterns in seven different states: air-dried (AD: original, Mg-saturated and K-saturated), saturated with ethylene glycol (EG) and glycerol (G), and heated at 300 and 550°C (Figure 2). Semiquantitative estimates for the main clay mineral groups of I/S (R = 0) and smectite (17–17.3 Å), illite (10 Å), and chlorite/kaolinite (7 Å) were carried out on the EG curve using the MacDiff software [*Petschick*, 2000] with the weighting factors introduced by *Biscaye* [1965]. For discrimination of kaolinite and chlorite, the (002) peak of kaolinite at 3.57 Å and the (004) peak of chlorite at 3.54 Å were analyzed through the slow XRD scan of the EG oriented mounts in the range from 24° to 26° 2θ at 0.0042° steps. Relative proportions of kaolinite and chlorite were determined based on the ratio from the 3.57/3.54 Å peak areas. The detailed methods and skills were preformed following the guidelines of *Zhang and Guo* [2014].

2.4. Major Elements Analyses

Thirty samples across the PETM were selected for major-element analyses to reveal the continental chemical weathering. In order to minimize the effects of grain size [*Yang et al.*, 2006] and carbonates on the chemical compositions, the powered samples were treated with 2 mol/L acetic acid to remove carbonates, and then the fine-grained fractions (<20 μm) [*Xiong et al.*, 2010] were separated according to Stoke's law for geochemical analyses. For X-ray fluorescence analysis, 0.5 g of fine-grained fractions (<20 μm) was heated to 1000°C in a muffle furnace, measuring the weight loss. The residue was then mixed with 5 g of dry $Li_2B_4O_7$, fused in a Pt crucible, and cooled as a glass disc. The prepared discs were measured on a Shimadzu XRF-1500 for major element concentrations at the IGG, CAS. Analytical uncertainties are ±2% for all major oxides except P_2O_5 and MnO for which uncertainties can be up to ±10%.

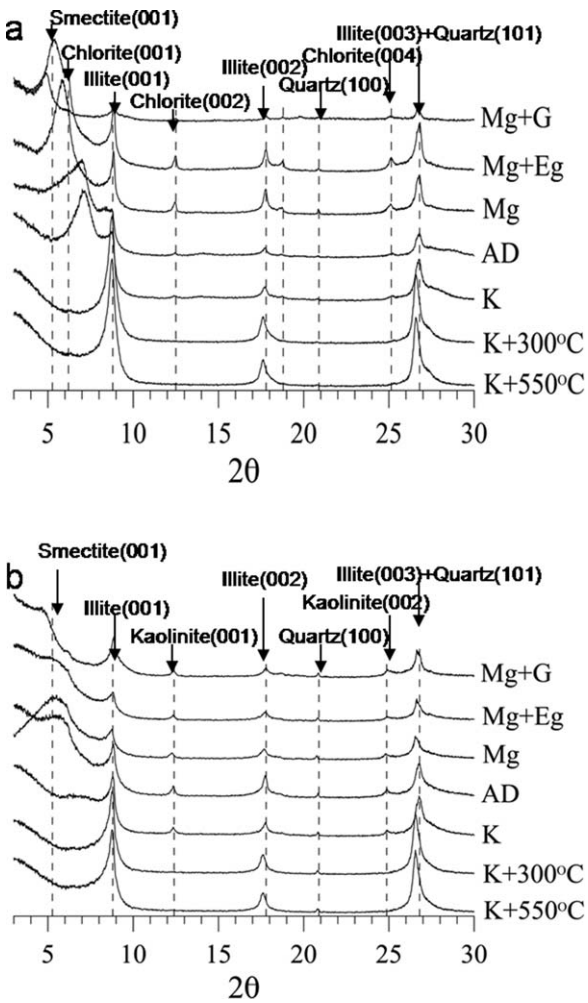

Figure 2. X-ray diffraction patterns of two typical samples. (a) The preexcursion sample; and (b) the excursion sample.

3. Results

3.1. Carbonate Geochemistry

Carbonate content ranges between 99.8% and 10.5% with an average of 81.3% over the whole section (Figure 3). Substantial fluctuations around 75% in carbonate content are observed before the CIE onset. Above this, the carbonate content generally shows a gradual decrease trend from a maximum (99.8%) at ~21 m to a minimum (10.5%) at ~34 m, coincident in trend with the change of $\delta^{13}C_{calcite}$ values, and then increases sharply to a value around 95% at ~40 m during the CIE recovery phase.

Our previous study shows extensive changes in carbonate minerals across the PETM [*Chen*

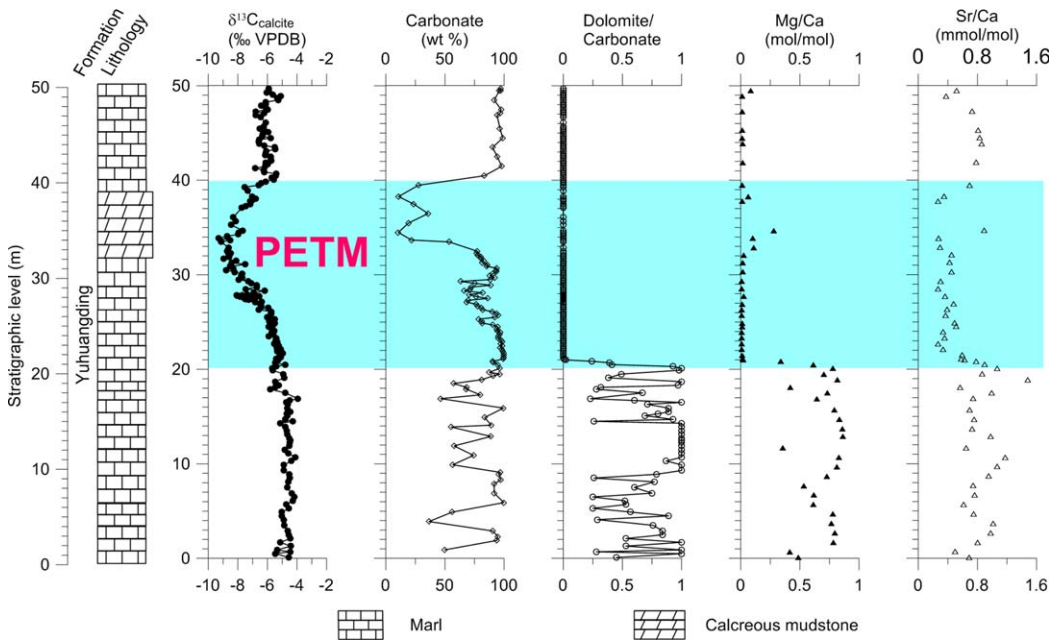

Figure 3. Mineral and elemental compositions of authigenic carbonates from the Nanyang basin. The blue-shaded area highlights the PETM. $\delta^{13}C_{calcite}$ data and Dolomite/Carbonate ratio are from *Chen et al*. [2014a].

et al., 2014a]. There exists abundant dolomite (28–100%) with a variable content of calcite in primary carbonates before the CIE. From the CIE onset, however, dolomite disappears and calcite is the only carbonate precipitate mineral for the remainder of the section (Figure 3).

Molar Mg/Ca ratios of carbonates broadly show similar change in trend to that in carbonate minerals (Figure 3). Before the CIE onset, Mg/Ca values fluctuate around 0.7 between 0 and 20 m, consistent with the existence of abundant dolomite. The Mg/Ca values then sharply decrease to close to 0, and keep relatively stable for the remainder of the section. Sr/Ca data fluctuate around a mean of 0.85 between 0 and 20 m, followed by an abrupt drop to a mean of 0.4 coeval with the CIE onset, and then increase to ~0.7 during the CIE recovery (Figure 3). The overall structure of the Sr/Ca data is similar to that of $\delta^{13}C_{calcite}$.

3.2. Clay Mineralogy

The mineralogical study of <2 μm subfractions reveals marked vertical changes in clay mineralogy at the Beigou sections (Figure 4). The clay fraction is dominated by smectite before the CIE onset, with subordinate illite, chlorite, and lack of kaolinite. A sudden appearance of kaolinite (from 0 to 5%) is synchronous with a gradual decrease in smectite, illite, and chlorite associated with the CIE onset. During the core of the CIE, the abundance of smectite and illite remains dominated, but the abundance of kaolinite increase to the maximum of 5% with scarce chlorite. The abundance of smectite and illite then increases while the kaolinite abundance decreases to a mean of 1% during the CIE recovery phase.

3.3. Major Elements and Weathering Index

A quantitative estimation of the degree of chemical weathering of the siliciclastic sediments is obtained by calculating the chemical index of alteration ($CIA = [Al_2O_3/(Al_2O_3 + CaO^* + Na_2O + K_2O)] \times 100$), where CaO* represents the calcium in the silicate fraction only [*Nesbitt and Young*, 1982]. The result is presented in Figure 5. Overall, the CIA values range between 65 and 83 with a mean of 75, suggesting moderate (CIA = 60–80) chemical weathering intensity. Concomitant with the onset of the CIE, the CIA values gradually increase to a peak value of 80 at 37 m, and then return to an average value (mean = 75) larger than the pre-CIE one (Figure 5).

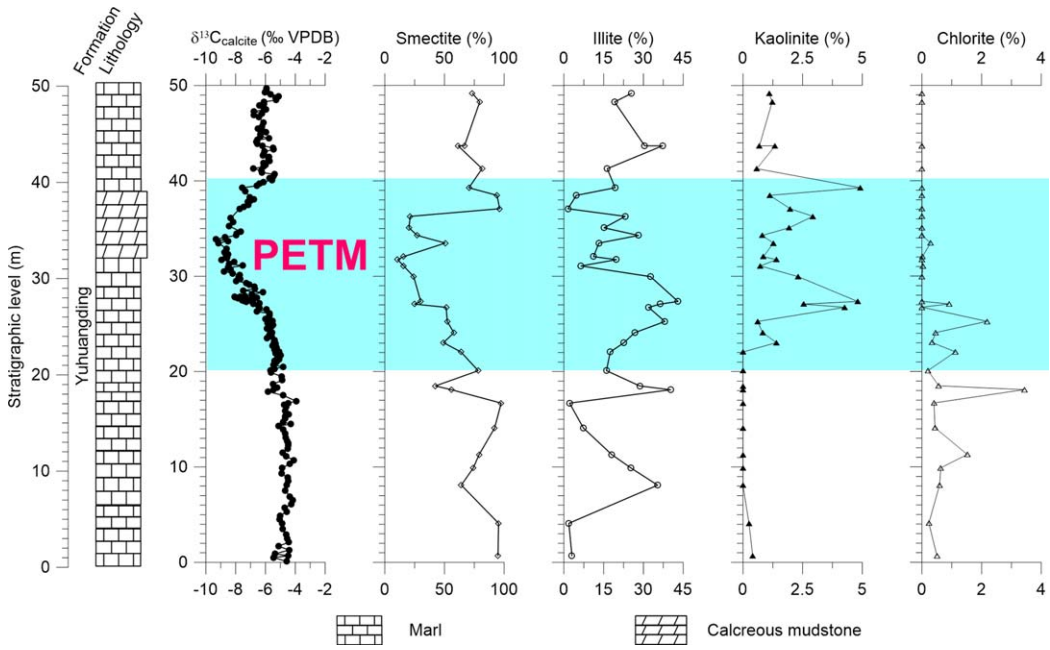

Figure 4. Clay mineral composition (%) of the Beigou section. The blue-shaded area highlights the PETM.

4. Interpretation

4.1. Carbonate Mineral Geochemistry

Authigenic carbonate minerals and their chemical composition in lacustrine settings are particularly useful geological proxies to inform about past ionic ratios, salinity of the lake water, and paleohydrology [*Mayayo et al.*, 1996; *Davis et al.*, 2008, 2009; *VanDeVelde and Bowen*, 2014]. The environmental signals may come from both the mineral phase of the carbonate mineral itself, indicative of salinity, and from Mg/Ca conditions within the lake water [*Müller et al.*, 1972]; they may be either in the form of minor element

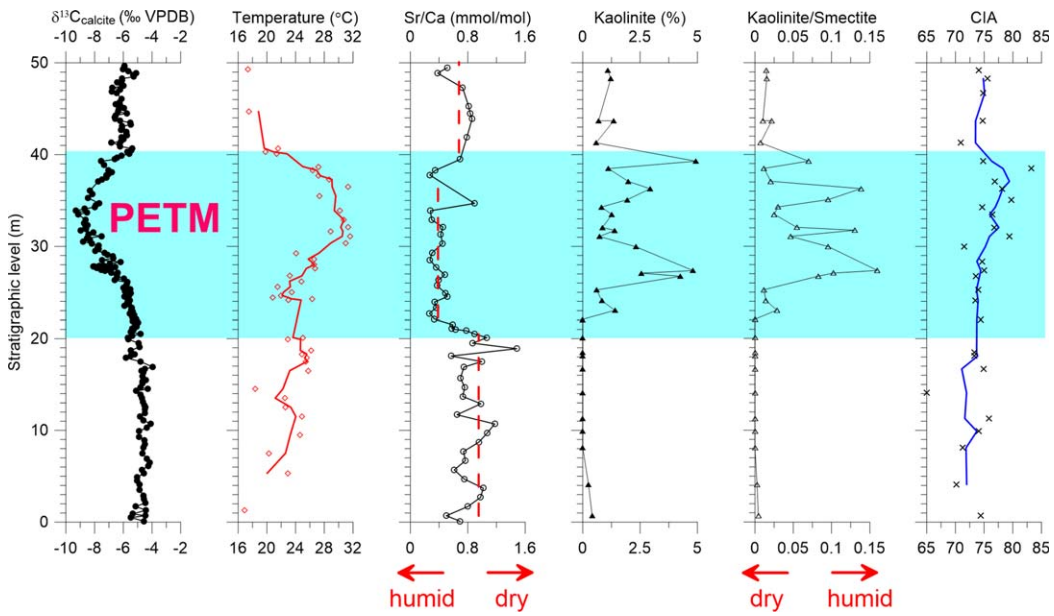

Figure 5. Combined diagram showing the regional climate change across the PETM in the Nanyang basin. The blue-shaded area highlights the PETM. $\delta^{13}C_{calcite}$ and temperature data are from *Chen et al.* [2014a]. The red (blue) solid line shows the three-points running average of red diamonds (black crosses).

concentrations (e.g., Sr/Ca) of the authigenic carbonates [*Chivas et al*., 1985]. At the Beigou section, the XRD analyses indicate that the dominant carbonate minerals in the samples are dolomite and calcite [*Chen et al*., 2014a]. Petrographic and mineralogical features have been provided as evidence for an authigenic origin of both carbonate minerals [*Chen et al*., 2014a].

It has long been recognized that the presence of authigenic dolomite in lacustrine deposits is suggestive of evaporative evolution of waterbody associated with more arid climatic episodes [*Müller et al*., 1972; *Last*, 1990; *Drummond et al*., 1996; *Dutkiewicz and von der Borch*, 1995]. In contrast, more calcitic micrites record a regionally positive hydrological balance between precipitation and evaporation, indicating that they formed as a primary precipitate during more humid climatic intervals corresponding to relative low salinities or lake freshening episodes [*Dutkiewicz and von der Borch*, 1995]. Recently, modern lakes investigation in northern China quantitatively explains the relationship between authigenic carbonate minerals and precipitation, and defines the rainfall thresholds of 600 and 400 mm for the formation of calcite and dolomite, respectively [*Gu et al*., 2015]. Thus, the abundance of dolomite at the Beigou section is interpreted to be a proxy of precipitation. Before the CIE onset, the existence of abundant dolomite (23–100%) is associated with highly evaporated lake water, implying that the regional precipitation is likely below 400 mm. Those stratigraphic intervals containing pure dolomicrite likely represent development of extremely arid climate and less precipitation. These results are broadly in line with previous paleoenvironmental reconstructions, which indicate an arid or semiarid climate setting in our study area during the Paleogene [*Sun and Wang*, 2005; *Guo et al*., 2008]. Coeval with the CIE onset and a gradual increase in temperature, dolomite disappears in the strata and calcite is the only carbonate mineral (Figures 3 and 5). The prominent change in carbonate mineral phase provides evidence for the lake freshening. Coupled with the increase in temperature, these results imply more regional precipitation across the PETM.

This interpretation of increased precipitation during the PETM is reinforced by the Mg/Ca and Sr/Ca molar ratios which show generally similar change in trend to carbonate mineral compositions (Figure 3). In general, the partitioning of Mg and Sr between host water and authigenic carbonate minerals is proportional to the ratio of these elements to Ca in the water [*Müller et al*., 1972; *Chivas et al*., 1985]. A negative precipitation-evaporation balance is manifested by an increase in Mg/Ca and Sr/Ca ratios as progressive evaporation of lake waters leads to more saline conditions [*Mayayo et al*., 1996; *Dutkiewicz et al*., 2000]. Therefore, the Mg/Ca and Sr/Ca ratios in the authigenic carbonates can be regarded as proxies for change in palaeosalinity in response to the ratio of precipitation to evaporation (P/E) [*Chivas et al*., 1985; *Yu and Ito*, 1999]. For the Beigou section, a prominent drop in Mg/Ca and Sr/Ca ratios at the CIE onset and persistent low values across the PETM demonstrate lake water freshened and less saline conditions, generally indicative of more precipitation during the PETM as suggested by the change in mineral phase of carbonate minerals. Collectively, climate aridity before the PETM, which is accompanied by an increase in Mg/Ca and Sr/Ca ratios in lake water, resulted in precipitation of abundant dolomite; in contrast, more precipitation across the PETM led to less saline conditions with a decrease in Mg/Ca and Sr/Ca ratios, and thus promoted the formation of calcite over dolomite. In addition, all proxies do not return to the pre-PETM values when the carbon isotope and temperature records indicate a termination of the event. These observations may imply a persistent long climatic state change after the carbon-cycle perturbation had stopped.

4.2. Formation of Clay Minerals and Paleoclimatic Significance

Since clay minerals in lacustrine sediments mainly supplied from weathered rocks represent a record of weathering conditions in the watershed, they have been demonstrated to be good indicator both of paleoclimate in the surrounding drainage area and of the diagenetic reactions taking place in the lake water [*Chamley*, 1989]. Diagenesis affecting clay minerals usually occur at burial depths exceeding 2 km [*Chamley*, 1998]. The thickness of the Cenozoic deposits within the Beigou section, however, does not exceed 2 km, suggesting that sediments did not suffer from deep burial diagenesis. Further evidence for low diagenetic overprint is documented by the following: (1) the lack of mixed-layered illite-smectite; (2) the constant but variable presence of smectite [*Bolle and Adatte*, 2001]. In addition, exhumation and reworking of the previously deposited soils are likely responsible for the change of clay minerals as suggested by the studies from many marginal marine sediments [*Thiry and Dupuis*, 2000; *Schmitz et al*., 2001]. The siliciclastic materials in the lacustrine sediments mainly come from the soils around the lake. If the kaolinite was inherited from the previously deposited soils, its abundance would show a synchronous change with the siliciclastic materials; however, the change in kaolinite in the Nanyang Basin is not coincided with the change of siliciclastic

materials as manifested by the abundance of carbonate. It also seems unimaginable that the previously deposited kaolinite-rich soils were hardly exhumed before the PETM when the kaolinite was absent in the sediments. Therefore, we explain the clay minerals and their relative abundance at the Beigou section as the regional information on paleoclimate.

Generally, illite and chlorite are considered common by-products of physical weathering with low hydrolysis typical of cool to temperate and/or dry climates [*Chamley*, 1989]. Smectite commonly develops abundantly in low reliefs where poor drainage prevents the removal of silica, alkaline, and alkaline-earth ions. This is generally linked to a warm climate with alternating humid and dry seasons [*Yemane et al*., 1987; *Chamley*, 1989]. In contrast, kaolinite is generally a by-product of highly hydrolytic weathering reactions and forms in perennially warm humid climates with a minimum temperature of 15°C [*Adatte et al*., 2002]. Therefore, the kaolinite/smectite ratio (K/SM) has been used a climate proxy that reflects humid/warm to more dry and seasonal climate variations [*Robert and Chamley*, 1991; *Adatte et al*., 2002; *Morales et al*., 2015].

In the Nanyang basin, the clay minerals before the CIE onset are characterized by high content in smectite and illite, and the low K/SM ratio with kaolinite nearly absent (Figures 4 and 5). These features of the clay mineral assemblages may indicate a weak chemical weathering and a relatively arid climate with alternating humid and dry seasons, which is in concert with the variable content of dolomite in the strata. The appearance and an increase in kaolinite marked the PETM, coeval with a gradual increase in temperature (Figure 5). This suggests that the climate during the PETM in the Nanyang basin is broadly dominated by warm, more humid conditions which favored intensive leaching of the parent rocks and formation of kaolinitic soils. The gradual decrease in smectite and the peak K/SM ratio across the PETM also further support increased precipitation and are associated with intensified chemical weathering of silicate. These results are overall in accordance with the paleoclimatic evolution inferred from the carbonate mineral geochemistry. Equally, the change of clay minerals extends well past the PETM $\delta^{13}C$ recovery phase (Figure 4), which seems to be in line with the argument that climatic state change persisted long after the approximately 200,000 year-long PETM with its increased carbon dioxide levels in the atmosphere [*Bornemann et al*., 2014].

5. Discussion and Implications

Although mean annual temperature is known to have increased globally during the PETM [*McInerney and Wing*, 2011; *Chen et al*., 2014a], precipitation patterns associated with the warming are complex and remain less well-understood. In North America midlatitude locations, paleosol, and paleobotanical features indicate that the climatic trend is toward more arid conditions during the PETM [*Wing et al*., 2005; *Kraus and Riggins*, 2007; *Woody et al*., 2014; *Kraus et al*., 2013]. In contrast, the high-latitude Arctic Ocean basin received more precipitation across the PETM inferred from δD record of higher-plant leaf wax lipids [*Pagani et al*., 2006]. Combining these observations with climate simulations [*Houghton et al*., 2001], several researchers suggested that precipitation was diverted from mid to high latitudes in response to CO_2-induced warming [*Pagani et al*., 2006; *Bowen and Bowen*, 2008]. As a corollary to this argument, subtropical areas would have to experience less mean precipitation. However, our study from the subtropical continent seems to argue against this interpretation. In the Nanyang basin, carbonate mineral geochemistry and clay mineral assemblages imply a change from a relatively arid climate with alternating humid and dry seasons during the latest Paleocene toward overall more humid conditions during the PETM. More humid conditions across the PETM could also be compatible with the anomalous larger CIE recorded in terrestrial organic substrates than that in marine records (Figure 1c) [*Bowen et al*., 2004; *Kohn*, 2010; *Chen et al*., 2014a]. The potential possibility for the increased precipitation in the continent may be linked to intense monsoonal-type rainfall or a slight northward shift of the intertropical convergence zone associated with the extreme PETM warming [*Shellito et al*., 2003; *Winguth et al*., 2010]. Recently, a moister climate is also inferred from *n*-alkane compound-specific hydrogen isotopic changes in midlatitude Europe [*Tipple et al*., 2011; *Garel et al*., 2013]. Collectively, the striking regional differences in precipitation imply that the response of the hydrological cycle to the PETM warming appears to be strongly dependent on the geographic position and corresponding climate zone.

In addition to the intense precipitation in the Nanyang basin, a prolonged period of climate state change has been observed in the geochemical proxies and clay mineral assemblages after the carbon-cycle perturbation had stopped (Figures 3 and 4). Similarly, the changes in fluvial deposition in North America and in

clay minerals in Europe have suggested persistent environmental perturbations well past the PETM recovery phase [*Foreman et al*., 2012; *Bornemann et al*., 2014]. Taken together, these observations probably demonstrate that a critical climate threshold may have been surpassed in response to the extreme PETM warming, which led to a new climate state in the hinterland that was not easily reversed after the close of the PETM [*Bornemann et al*., 2014].

Following the rapid input of huge CO_2 at its onset, the PETM lasts for ~170 kyr [*Röhl et al*., 2007; *Charles et al*., 2011], a period during which the released CO_2 was gradually sequestered. One of the proposed possibilities for permanently sequestering carbon and lowering atmospheric CO_2 levels is the enhanced chemical weathering of silicate rocks and pedogenesis on the continents [*Zachos and Dickens*, 2000]. So far, most reports about intensified weathering are indirectly from marine sediments [*Ravizza et al*., 2001; *Kelly et al*., 2005; *Dallanave et al*., 2010], whereas the only terrestrial records are from North America [*Clechenko et al*., 2007; *Kraus and Riggins*, 2007; *White and Schiebout*, 2008]. In this study, the evolution of major-element contents and clay minerals provides another direct terrestrial evidence to attest the silicate-weathering mechanism. In general, warmer and more humid climate is favorable for the weathering of the continental crust. Ca, Na, and K are removed by soil solutions whereas Al increases in the weathering product [*Nesbitt and Young*, 1982, 1984]. The weathering signal including in these major-element contents is generally embodied in the CIA index, which is the molar ratio between aluminium oxide and the sum of aluminium and more labile oxides [*Nesbitt and Young*, 1982]. In the Nanyang basin, a gradual increase in CIA values is associated with the carbon isotope excursion and the PETM warming (Figure 5). This observation suggests an increased silicate chemical weathering in the watershed during the PETM that would have resulted from an increase in humidity and soil CO_2. The appearance and an increase in kaolinite at the expense of smectite also imply an intensified pedogenesis, further in support of enhanced chemical weathering in response to warmer and more humid climate in the continent. These results are in line with that recorded in North America where increased pedogenesis has been observed across the PETM [*Clechenko et al*., 2007; *White and Schiebout*, 2008]. As a corollary, accelerated silicate weathering will deliver more soluble calcium and magnesium cations to the oceans by river runoff, which should deepen the lysocline of carbonate. Indeed, the pattern of carbonate sedimentation recovered from the Walvis Ridge and the Site 690 is compatible with such a deepening of the lysocline; carbonate content in the sediments within the CIE recovery phase is higher than in the pre-CIE interval [*Zachos et al*., 2005; *Kelly et al*., 2010]. Overall, our geochemical and mineralogical proxies from the terrestrial sediments support the hypothesis that enhanced continental silicate weathering and pedogenisis helped sequester carbon across the PETM [*Zachos and Dickens*, 2000; *Zachos et al*., 2005]. In addition, the persistent higher CIA values after the close of the PETM further suggest a prolonged environmental perturbation in the continental settings.

6. Conclusions

The lacustrine sediments recovered from the Nanyang basin provide the first opportunity to evaluate the response of the local precipitation pattern and weathering during the PETM in China interior. Geochemical and mineralogical proxies suggest a general increase in precipitation associated with the PETM in central China, in contrast to a drier climate recorded in North America [*Wing et al*., 2005; *Kraus and Riggins*, 2007; *Woody et al*., 2014; *Kraus et al*., 2013]. These results collectively demonstrate that the precipitation patterns in response to the PETM warming are complex, and strongly dependent on the geographic position and corresponding climate zone. The relatively humid conditions persisted long after the close of the PETM, implying that the transient hyper-greenhouse climate may have forced the regional climate system into a new climate state that was not easily reversed. In addition, a gradual increase in CIA values and the appearance of kaolinite are coeval with the PETM onset, suggestive of an enhanced continental weathering/pedogenesis in response to warmer and more humid climate in the watershed. This corroborates the theory that an accelerated silicate weathering helped sequester carbon and lower the atmospheric greenhouse-gas levels during the PETM.

Acknowledgments
This work was supported by the Strategic Priority Research Program of the Chinese Academy of Sciences (grand XDB03020503), the (973) National Basic Research Program of China (grand 2013CB956404 and 2012CB821905), and the China Postdoctoral Science Foundation (grand 2015M570143). We thank Bin Hu and Dingshuai Xue for their assistance in data measurement, and Zihua Tang for the field sampling. We also thank two anonymous reviewers for their helpful comments. Data supporting the paper is available in supporting information.

References

Adatte, T., G. Keller and W. Stinnesbeck (2002), Late Cretaceous to early Paleocene climate and sea-level fluctuations: the Tunisian record, *Palaeogeogr. Palaeoclimatol. Palaeoecol.*, *178*, 165–196.

Biscaye, B. E. (1965), Mineralogy and sedimentation of recent deep-sea clay in the Atlantic ocean and adjacent seas and oceans, *Geol. Soc. Am. Bull.*, *76*, 803–832.
Bolle, M. P., and T. Adatte (2001), Palaeocene-early Eocene climatic evolution in the Tethyan realm: Clay mineral evidence, *Clay Miner.*, *36*, 249–261.
Bornemann, A., R. D. Norris, J. A. Lyman, S. D'haenens, J. Groeneveld, U. Röhl, K. A. Farley, and R. P. Speijer (2014), Persistent environmental change after the Paleocene–Eocene Thermal Maximum in the eastern North Atlantic, *Earth Planet. Sci. Lett.*, *394*, 70–81.
Bowen, G. J., and B. B. Bowen (2008), Mechanisms of PETM global change constrained by a new record from central Utah, *Geology*, *36*, 379–382.
Bowen, G. J., D. J. Beerling, P. L. Koch, J. C. Zachos, and T. Quattlebaum (2004), A humid climate state during the Palaeocene/Eocene thermal maximum, *Nature*, *432*, 495–499.
Chamley, H. (1989), *Clay Sedimentology*, Spring, Berlin.
Chamley, H. (1998), Clay mineral sedimentation in the Ocean, in *Soils and Sediments (Mineralogy and Geochemistry)*, edited by H. Paquet and N. Clauer, pp. 269–302, Springer, Berlin.
Charles, A. J., D. J. Condon, I. C. Harding, H. Pälike, J. E. A. Marshall, Y. Cui, L. Kump, and I. W. Croudace (2011), Constraints on the numerical age of the Paleocene-Eocene boundary, *Geochem. Geophys. Geosyst.*, *12*, Q0AA17, doi:10.1029/2010GC003426.
Chen, Z., X. Wang, J. Hu, S. Yang, M. Zhu, X. Dong, Z. Tang, P. Peng, and Z. Ding (2014a), Structure of the carbon isotope excursion in a high-resolution lacustrine Paleocene-Eocene Thermal Maximum record from central China, *Earth Planet. Sci. Lett.*, *408*, 331–340.
Chen, Z., Z. Ding, Z. Tang, X. Wang, and S. Yang (2014b), Early Eocene carbon isotope excursions: Evidence from the terrestrial coal seam in the Fushun Basin, Northeast China, *Geophys. Res. Lett.*, *41*, 3559–3564, doi:10.1002/2014GL059808.
Chivas, A. R., P. De Deckker, and J. M. G. Shelley (1985), Strontium content of ostracods indicates lacustrine palaeosalinity, *Nature*, *316*, 251–253.
Clechenko, E. R., D. C. Kelly, G. J. Harrington, and C. A. Stiles (2007), Terrestrial records of a regional weathering profile at the Paleocene-Eocene boundary in the Williston Basin of North Dakota, *Geol. Soc. Am. Bull.*, *119*, 428–442.
Dallanave, E., L. Tauxe, G. Muttoni, and D. Rio (2010), Silicate weathering machine at work: Rock magnetic data from the late Paleocene-early Eocene Cicogna section, Italy, *Geochem. Geophys. Geosyst.*, *11*, Q07008, doi:10.1029/2010GC003142.
Davis, S. J., B. A. Wiegand, A. R. Carroll, and C. P. Chamberlain (2008), The effect of drainage reorganization on paleoaltimetry studies: An example from the Paleogene Laramide foreland, *Earth Planet. Sci. Lett.*, *275*, 258–268.
Davis, S. J., A. Mulch, A. R. Carroll, T. W. Horton, and C. P. Chamberlain (2009), Paleogene landscape evolution of the central North American Cordillera: Developing topography and hydrology in the Laramide foreland, *Geol. Soc. Am. Bull.*, *121*, 100–116.
Dickens, G. R., J. R. O'neil, D. K. Rea, and R. M. Owen (1995), Dissociation of oceanic methane hydrate as a cause of the carbon isotope excursion at the end of the Paleocene, *Paleoceanography*, *10*, 965–971.
Drummond, C. N., B. H. Wilkinson, and K. C. Lohmann (1996), Climatic control of fluvial-lacustrine cyclicity in the Cretaceous Cordilleran Foreland Basin, western United States, *Sedimentology*, *43*, 677–689.
Dutkiewicz, A., and C. C. von der Borch (1995), Lake Greenly, Eyre Peninsula, South Australia: Sedimentology, palaeoclimatic and palaeohydrologic cycles, *Palaeogeogr. Palaeoclimatol. Palaeoecol.*, *113*, 43–56.
Dutkiewicz, A., A. L. Herczeg, and J. C. Dighton (2000), Past changes to isotopic and solute balances in a continental playa: Clues from stable isotopes of lacustrine carbonates, *Chem. Geol.*, *165*, 309–329.
Feng, Z., S. Zhou, J. Wang, and B. Gu (1997), The changes of Meso-Cenozoic Paleogeographic environments in the southwest of Henan, *Henan Geol.*, *12*, 270–277.
Feng, Z., S. Zhou, and Z. Li (1999), The age of the late cretaceous red beds in southwestern Henan Provence, *Reg. Geol. China*, *3*, 320–328.
Foreman, B. Z., P. L. Heller, and M. T. Clementz (2012), Fluvial response to abrupt global warming at the Palaeocene/Eocene boundary, *Nature*, *491*, 92–95.
Garel, S., et al. (2013), Paleohydrological and paleoenvironmental changes recorded in terrestrial sediments of the Paleocene-Eocene boundary (Normandy, France), *Palaeogeogr. Palaeoclimatol. Palaeoecol.*, *376*, 184–199.
Gu, N., W. Y. Jiang, L. Wang, E. L. Zhang, S. L. Yang, and S. F. Xiong (2015), Rainfall thresholds for the precipitation of carbonate and evaporite minerals in modern lakes in northern China, *Geophys. Res. Lett.*, *42*, 5895–5901, doi:10.1002/2015GL064340.
Guo, Z. T., et al. (2008), A major reorganization of Asian climate by the early Miocene, *Clim. Past*, *4*, 153–174.
Held, I. M., and B. J. Soden (2006), Robust responses of the hydrological cycle to global warming, *J. Clim.*, *19*, 5686–5699.
Hollis, C. J., G. R. Dickens, B. D. Field, C. M. Jones, and C. Percy Strong (2005), The Paleocene-Eocene transition at Mead Stream, New Zealand: A southern Pacific record of early Cenozoic global change, *Palaeogeogr. Palaeoclimatol. Palaeoecol.*, *215*, 313–343.
Houghton, J. T., Y. Ding, D. J. Griggs, M. Noguer, P. J. van der Linden, X. Dai, K. Maskell, and C. A. Johnson (Eds.) (2001), *Climate Change 2001: The Scientific Basis*, 881 pp., Cambridge Univ. Press, N. Y.
John, C. M., S. M. Bohaty, J. C. Zachos, A. Sluijs, S. Gibbs, H. Brinkhuis, and T. J. Bralower (2008), North American continental margin records of the Paleocene-Eocene thermal maximum: Implications for global carbon and hydrological cycling, *Paleoceanography*, *23*, PA2217, doi:10.1029/2007PA001465.
Kelly, D. C., J. C. Zachos, T. J. Bralower, and S. A. Schellenberg (2005), Enhanced terrestrial weathering/runoff and surface ocean carbonate production during the recovery stages of the Paleocene-Eocene thermal maximum, *Paleoceanography*, *20*, PA4023, doi:10.1029/2005PA001163.
Kelly, D. C., T. M. J. Nielsen, H. K. McCarren, J. C. Zachos, and U. Röhl (2010), Spatiotemporal patterns of carbonate sedimentation in the south Atlantic: Implications for carbon cycling during the paleocene-eocene thermal maximum, *Palaeogeogr. Palaeoclimatol. Palaeoecol.*, *293*, 30–40.
Kennett, J. P., and L. C. Stott (1991), Abrupt deep-sea warming, palaeoceanographic changes and benthic extinctions at the end of the Palaeocene, *Nature*, *353*, 225–229.
Kohn, M. J. (2010), Carbon isotope compositions of terrestrial C3 plants as indicators of (paleo)ecology and (paleo)climate, *Proc. Natl. Acad. Sci. U. S. A.*, *107*, 19,691–19,695.
Kraus, M. J., and S. Riggins (2007), Transient drying during the Paleocene-Eocene Thermal Maximum (PETM): Analysis of paleosols in the bighorn basin, Wyoming, *Palaeogeogr. Palaeoclimatol. Palaeoecol.*, *245*, 444–461.
Kraus, M. J., F. A. McInerney, S. L. Wing, R. Secord, A. A. Baczynski, and J. I. Bloch (2013), Paleohydrologic response to continental warming during the Paleocene-Eocene Thermal Maximum, Bighorn Basin, Wyoming, *Palaeogeogr. Palaeoclimatol. Palaeoecol.*, *370*, 196–208.
Last, W. M. (1990), Lacustrine dolomite-an overview of modern, Holocene, and Pleistocene occurrences, *Earth Sci. Rev.*, *27*, 221–263.
Ma, A., and J. Cheng (1991), On biostratigraphical subdivision of Yuhuangding formation in Liguanqiao Basin of eastern Qinling region, *Sci. Geol. Sin.*, *1*, 21–29.

Mayayo, M. J., B. Bauluz, A. López-Galindo, and J. M. González-López (1996), Mineralogy and geochemistry of the carbonates in the Calatayud Basin (Zaragoza, Spain), *Chem. Geol.*, *130*, 123–136.

McInerney, F. A., and S. L. Wing (2011), The paleocene-eocene thermal maximum: A perturbation of carbon cycle, climate, and biosphere with implications for the future, *Annu. Rev. Earth Planet. Sci.*, *39*, 489–516.

Meissner, K. J., T. J. Bralower, K. Alexander, T. D. Jones, W. Sijp, and M. Ward (2014), The Paleocene-Eocene Thermal Maximum: How much carbon is enough? *Paleoceanography*, *29*, 946–963, doi:10.1002/2014PA002650.

Morales, C., A. Kujau, U. Heimhofer, J. Mutterlose, J. E. Spangenberg, T. Adatte, I. Ploch, and K. B. Föllmi (2015), Palaeoclimate and palaeoenvironmental changes through the onset of the Valanginian carbon-isotope excursion: Evidence from the Polish Basin, *Palaeogeogr. Palaeoclimatol. Palaeoecol.*, *426*, 183–198.

Müller, G., G. Irion, and U. Förstner (1972), Formation and diagenesis of inorganic Ca-Mg carbonate in the lacustrine environment, *Naturwissenschaften*, *59*, 158–164.

Nesbitt, H. W., and G. M. Young (1982), Early Proterozoic climates and plate motions inferred from major element chemistry of lutites, *Nature*, *299*, 715–717.

Nesbitt, H. W., and G. M. Young (1984), Prediction of some weathering trends of plutonic and volcanic rocks based on thermodynamic and kinetic considerations, *Geochim. Cosmochim. Acta*, *48*, 1523–1534.

Pagani, M., N. Pedentchouk, M. Huber, A. Sluijs, S. Schouten, H. Brinkhuis, J. S. S. Damsté, G. R. Dickens and the Expedition 302 Scientists (2006), Arctic hydrology during global warming at the Palaeocene/Eocene thermal maximum, *Nature*, *442*, 671–675.

Petschick, R. (2000), MacDiff 4.2.2 [Online].[Available at http://servermac.geologie.un-frankfurt.de/Rainer.html.]

Pierrehumbert, R. T. (2002), The hydrologic cycle in deep-time climate problems, *Nature*, *419*, 191–198.

Ravizza, G., R. N. Norris, J. Blusztajn, and M. P. Aubry (2001), An osmium isotope excursion associated with the late Paleocene thermal maximum: Evidence of intensified chemical weathering, *Paleoceanography*, *16*, 155–163.

Robert, C., and H. Chamley (1991), Development of early Eocene warm climates, as inferred from clay mineral varations in oceanic sediments, *Palaeogeogr. Palaeoclimatol. Palaeoecol.*, *89*, 315–332.

Robert, C., and J. P. Kennett (1994), Antarctic subtropical humid episode at the Paleocene-Eocene boundary: Clay-mineral evidence, *Geology*, *22*, 211–214.

Röhl, U., T. Westerhold, T. J. Bralower, and J. C. Zachos (2007), On the duration of the Paleocene-Eocene thermal maximum (PETM), *Geochem. Geophys. Geosyst.*, *8*, Q12002, doi:10.1029/2007GC001784.

Schmitz, B., and V. Pujalte (2003), Sea-level, humidity, and land-erosion records across the initial Eocene thermal maximum from a continental-marine transect in northern Spain, *Geology*, *31*, 689–692.

Schmitz, B., and V. Pujalte (2007), Abrupt increase in seasonal extreme precipitation at the Paleocene-Eocene boundary, *Geology*, *35*, 215–218.

Schmitz, B., V. Pujalte, and K. Nunez-Betelu (2001), Climate and sea-level perturbations during the initial Eocene thermal maximum: Evidence from siliciclastic units in the Basque Basin (Ermua, Zumaia, and Trabakua Pass), northern Spain, *Palaeogeogr. Palaeoclimatol. Palaeoecol.*, *165*, 299–320.

Shellito, C. J., L. C. Sloan, and M. Huber (2003), Climate model sensitivity to atmospheric CO_2 levels in the Early-Middle Paleogene, *Palaeogeogr. Palaeoclimatol. Palaeoecol.*, *193*, 113–123.

Sluijs, A., et al. (2006), Subtropical arctic ocean temperatures during the Palaeocene/Eocene thermal maximum, *Nature*, *441*, 610–613.

Sun, X. J., and P. C. Wang (2005), How old is the Asian monsoon system?-Palaeobotanical records from China, *Palaeogeogr. Palaeoclimatol. Palaeoecol.*, *222*, 181–222.

Thiry, M., and M. Dupuis (2000), Use of clay minerals for paleoclimatic reconstructions: Limits of the method with special reference to the Paleocene-lower Eocene interval, *GFF*, *122*,166–167.

Thomas, D. J., T. J. Bralower, and J. C. Zachos (1999), New evidence for subtropical warming during the late Paleocene thermal maximum: Stable isotopes from Deep Sea Drilling Project Site 527, Walvis Ridge, *Paleoceanography*, *14*, 561–570.

Ting, S. Y., G. J. Bowen, P. L. Koch, W. C. Clyde, Y. Wang, Y. Wang, and M. C. McKenna (2003), Biostratigraphic, chemostratigraphic, and magnetostratigraphic study across the Paleocene-Eocene boundary in the Hengyang Basin, Hunan, China, in *Causes and Consequences of Globally Warm Climates in the Early Paleogene*, edited by S. L. Wing et al., pp. 521–535, Geol. Soc. Am., Boulder, Colo.

Tipple, B. J., M. Pagani, S. Krishnan, S. S. Dirghangi, S. Galeotti, C. Agnini, L. Giusberti, and D. Rio (2011), Coupled high-resolution marine and terrestrial records of carbon and hydrologic cycles variations during the Paleocene-Eocene Thermal Maximum (PETM), *Earth Planet. Sci. Lett.*, *311*, 82–92.

Trenberth, K. E. (2011), Changes in precipitation with climate change, *Clim. Res.*, *47*, 1–16.

Tripati, A., and H. Elderfield (2005), Deep-sea temperature and circulation changes at the Paleocene-Eocene thermal maximum, *Science*, *308*, 1894–1898.

VanDeVelde, J. H., and G. J. Bowen (2014), Isotope hydrology of early paleogene Lake Flagstaff, central Utah: Implications for Cordilleran evolution, *Am. J. Sci.*, *314*, 1436–1461.

Wang, E., Q. C. Meng, B. C. Burchfiel, and G. Zhang (2003), Mesozoic large-scale lateral extrusion, rotation, and uplift of the Tongbai–Dabie Shan belt in east China, *Geology*, *31*, 307–310.

Weijers, J. W. H., S. Schouten, A. Sluijs, H. Brinkhuis, and J. S. S. Damsté (2007), Warm arctic continents during the Palaeocene-Eocene thermal maximum, *Earth Planet. Sci. Lett.*, *261*, 230–238.

White, P. D., and J. Schiebout (2008), Paleogene paleosols and changes in pedogenesis during the initial Eocene thermal maximum: Big Bend National Park, Texas, USA, *Geol. Soc. Am. Bull.*, *120*, 1347–1361.

Wing, S. L., G. J. Harrington, F. A. Smith, J. I. Bloch, D. M. Boyer, and K. H. Freeman (2005), Transient floral change and rapid global warming at the Paleocene-Eocene boundary, *Science*, *310*, 993–996.

Winguth, A., C. Shellito, C. Shields, and C. Winguth (2010), Climate Response at the paleocene-eocene thermal maximum to greenhouse gas forcing: A model study with CCSM3, *J. Clim.*, *23*, 2562–2583.

Woody, D. T., J. J. Smith, M. J. Kraus, and S. T. Hasiotis (2014), Manganese-bearing rhizocretions in the Willwood Formation, Wyoming, U. S. A.: Implications for paleoclimate during the Paleocene-Eocene Thermal Maximum, *Palaios*, *29*, 266–276.

Xiong, S. F., Z. L. Ding, Y. J. Zhu, R. Zhou, and H. J. Lu (2010), A ~6 Ma chemical weathering history, the grain size dependence of chemical weathering intensity, and its implications for provenance change of the Chinese loess-red clay deposit, *Quat. Sci. Rev.*, *29*, 1911–1922.

Yang, S. L., F. Ding, and Z. L. Ding (2006), Pleistocene chemical weathering history of Asian arid and semi-arid regions recorded in loess deposits of China and Tajikistan, *Geochim. Cosmochim. Acta*, *70*, 1695–1709.

Yang, S. L, Z. L. Ding, Y. Y. Li, X. Wang, W. Y. Jiang, and X. F. Huang (2015), Warming-induced northwestward migration of the East Asian monsoon rain belt from the Last Glacial Maximum to the mid-Holocene, *Proc. Natl. Acad. Sci. U. S. A.*, *112*, 13,178–13,183.

Yemane, K., C. Robert, and R. Bonnefille (1987), Pollen and clay mineral assemblages of a late miocene lacustrine sequence from the northwestern ethiopian highlands, *Palaeogeogr. Palaeoclimatol. Palaeoecol.*, *60*, 123–141.

Yu, Z., and E. Ito (1999), Possible solar forcing of century-scale drought frequency in the northern Great Plains, *Geology*, *27*, 263–266.

Zachos, J. C., and G. R. Dickens (2000), An assessment of the biogeochemical feedback response to the climatic and chemical perturbations of the LPTM, *GFF*, *122*, 188–189.

Zachos, J. C., M. W. Wara, S. Bohaty, M. L. Delaney, M. R. Petrizzo, A. Brill, T. J. Bralower, and I. Premoli-Silva (2003), A transient rise in tropical sea surface temperature during the Paleocene-Eocene Thermal Maximum, *Science*, *302*, 1551–1554.

Zachos, J. C., et al. (2005), Rapid acidification of the ocean during the Paleocene-Eocene thermal maximum, *Science*, *308*, 1611–1615.

Zachos, J. C., G. R. Dickens, and R. E. Zeebe (2008), An early Cenozoic perspective on greenhouse warming and carbon-cycle dynamics, *Nature*, *451*, 279–283.

Zeebe, R. E., J. C. Zachos, and G. R. Dickens (2009), Carbon dioxide forcing alone insufficient to explain Palaeocene-Eocene Thermal Maximum warming, *Nat. Geosci.*, *2*, 576–580.

Zhang, C. X., and Z. T. Guo (2014), Clay mineral changes across the Eocene–Oligocene transition in the sedimentary sequence at Xining occurred prior to global cooling, *Palaeogeogr. Palaeoclimatol. Palaeoecol.*, *411*, 18–29.

Zhu, M., Z. Ding, X. Wang, Z. Chen, H. Jiang, X. Dong, J. Ji, Z. Tang and P. Luo (2010), High-resolution carbon isotope record for the Paleocene-Eocene thermal maximum from the Nanyang Basin, Central China, *Chin. Sci. Bull.*, *55*, 3606–3611.